

Type-II Weyl nodes, flat bands, and evidence for a topological Hall-effect in the new ferromagnet FeCr_3Te_6

Shyam Raj Karullithodi^{1,2}, Vadym Kulichenko¹, Mario A. Plata³, Andrzej Ptok⁴, Sang-Eon Lee¹, Gregory T. McCandless³, Julia Y. Chan³, and Luis Balicas^{1,2,*}

¹*National High Magnetic Field Laboratory, 1800 E. Paul Dirac Dr., Tallahassee, Florida 32310, USA*

²*Department of Physics, Florida State University, 77 Chieftan Way, Tallahassee, Florida 32306, USA*

³*Department of Chemistry and Biochemistry, Baylor University, Waco, Texas 76798, USA*

⁴*Institute of Nuclear Physics, Polish Academy of Sciences, PL-31342 Krakow, Poland*

 (Received 21 November 2024; revised 5 February 2025; accepted 4 April 2025; published 18 April 2025)

The interplay between linearly dispersing, or Dirac-like, and flat electronic bands, for instance, in the kagome ferromagnets, has attracted attention due to a possible interplay between topology and electronic correlations. Here, we report the synthesis, structural, electrical, and magnetic properties of a single-crystalline ferromagnetic compound, namely $\text{Fe}_{1/3}\text{CrTe}_2$ or FeCr_3Te_6 , which crystallizes in the $P\bar{3}m1$ space group instead of the $I2/m$ previously reported for FeCr_2Te_4 . Electronic band structure calculations reveal type-II Dirac nodes and relatively flat bands near the Fermi level (ε_F). This compound shows onset Curie temperature $T_c \simeq 120$ K, followed by an additional ferromagnetic transition near $T_{c2} \sim 92.5$ K. Below T_c , FeCr_3Te_6 displays a pronounced anomalous Hall effect, as well as sizable coercive fields that exceed $\mu_0 H = 1$ T at low T s. However, a scaling analysis indicates that the anomalous Hall effect results from a significant intrinsic contribution, as expected from the calculations, and also from the extrinsic mechanism, i.e., scattering. The extrinsic contribution probably results from occupational disorder at the 1b Fe-site within the van der Waals gap of the CrTe_2 host. We also observe evidence for a topological Hall component superimposed onto the overall Hall response, suggesting the presence of chiral spin textures akin to skyrmions in this centrosymmetric system. Their possible presence will require experimental confirmation.

DOI: [10.1103/PhysRevMaterials.9.044203](https://doi.org/10.1103/PhysRevMaterials.9.044203)

I. INTRODUCTION

The search for rare-earth-free ferromagnets is an endeavor of current technological importance [1,2]. Topological magnetic compounds are predicted to support chiral electronic channels with perfect conduction, which could be used for an array of applications, ranging from information storage to dissipationless charge and spin transport [3]. A notable example is the quantum anomalous Hall effect observed on the surface of topological insulators once the Dirac node is gapped via the introduction of magnetic impurities [4,5].

The Hall response of ferromagnets is frequently characterized by several contributions, i.e., the conventional Hall, the anomalous Hall [6], and the topological Hall effect [7]. The conventional Hall response results from the Lorentz force acting on the charge carriers and deflecting their trajectories under a magnetic field. The anomalous Hall effect (AHE), on the other hand, occurs in broken time-reversal symmetry systems, e.g., ferromagnets, as a consequence of the spin-orbit coupling [8]. Karpus and Luttinger [9] showed that under an external electric field, electrons acquire an additional contribution to their group velocity or an anomalous velocity perpendicular to the electric field that contributes to the Hall response. In ferromagnetic conductors, the sum of this anomalous velocity over all occupied bands can be

nonzero, implying a net contribution to the Hall conductivity σ_{xy} . Since this contribution depends solely on the material's band structure, it is referred to as the intrinsic contribution to the AHE. The intrinsic mechanism can be interpreted as a manifestation of the Berry phase acting on the Bloch state of the charge carriers [10,11]. We must also mention scattering-related contributions to the AHE, namely the side jump and the skew-scattering mechanisms. The former results from electron velocities that are deflected in opposite directions by the opposite electric fields acting on them upon approaching and leaving an impurity [12]. The latter results from electrons asymmetrically scattered by impurities due to the spin-orbit interaction, which causes electrons with different spins to scatter in different directions [13,14].

Here, we report on a new member of the FeCr_2X_4 (where X is a chalcogen) family of compounds, which are said to be characterized by a competition between spin-orbit coupling and exchange interactions [15,16]. For example, FeCr_2S_4 and FeCr_2Se_4 are insulators, with the former compound reported to become a ferrimagnet below $T_c = 165$ K [17,18], and the latter an antiferromagnet at $T_N = 218$ K displaying small moment ferrimagnetism below 75 K [19,20]. In contrast, FeCr_2Te_4 , which is derived from Cr_3Te_4 and crystallizes in the space group $I2/m$, is reported to be metallic [21] and to display an Ising-like ferrimagnetic state with a Curie temperature $T_c \simeq 124$ K [16]. This compound displays an anomalous Hall response $\rho_{xy}^A \propto \rho_{xx}$, implying that it is in the dirty regime and likely dominated by the skew-scattering mechanism [21].

*Contact author: balicas@magnet.fsu.edu

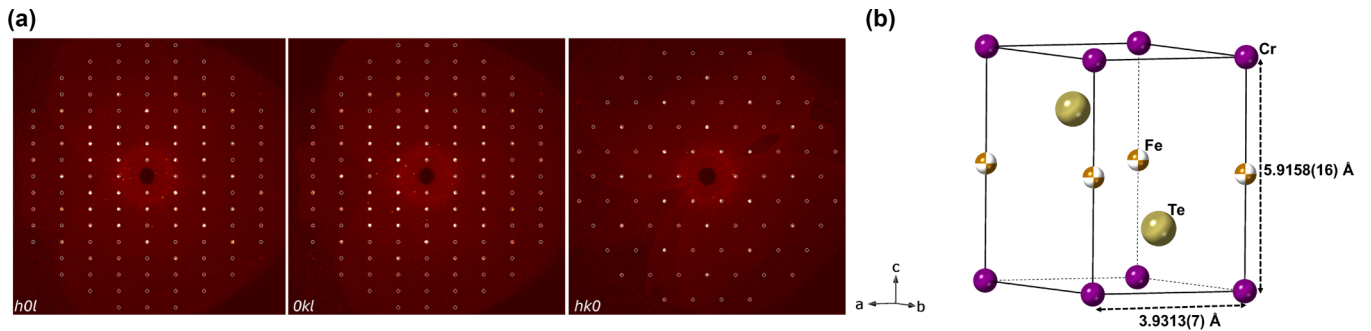


FIG. 1. (a) Indexed precession images of X-ray diffraction collected along the $h0l$, $0kl$, and $hk0$ planes, used to refine its crystallographic structure. (b) Crystal structure and lattice parameters of FeCr_3Te_6 .

The compound synthesized herein crystallizes in the space group $P\bar{3}m1$ with the nominal composition $\text{Fe}_{1/3}\text{CrTe}_2$ and can be seen as another intercalated variant of CrTe_2 , but with random Fe distribution. In this manuscript, we provide a detailed structural analysis, concomitant band structure calculations, and the study of the band structure's magnetic and electrical transport properties. Band structure calculations reveal relatively flat bands near the Fermi level ε_F coexisting with a type-II Dirac/Weyl node located precisely at ε_F . Type-II Weyl node(s) would be stabilized by two ferromagnetic transitions observed upon cooling. A scaling analysis of its anomalous Hall effect indeed points to a sizeable intrinsic contribution (Berry phase dominated) albeit subjected to extrinsic contributions from scattering mechanisms, likely resulting from structural disorder. Remarkably, despite the centrosymmetric nature of this compound, we find evidence for a topological Hall signal at low temperatures, once the anomalous Hall component is subtracted from the raw Hall signal. This suggests the possible existence of non-co-planar spin textures, such as skyrmions.

II. RESULTS

A. Synthesis

We grew single crystals of $\text{Fe}_{1/3}\text{CrTe}_2$ via a solid-state reaction followed by a chemical vapor transport (CVT) method. High-purity Fe, Cr, and Te powders in the 1:3:6 ratio were loaded into an evacuated quartz ampoule and subsequently sealed. The ampoule was placed in a furnace, heated to 900°C , and maintained at this temperature for 24 hours. The product was then ground in an agate mortar. For single-crystal growth, the powder was reintroduced into an ampoule, with 100 mg of I_2 as the transport agent. Subsequently, the evacuated ampoule was placed into a two-zone tubular furnace, with the temperature of the source kept at 760°C and that of the crystallization zone at 700°C , for seven days. As the final step, the quartz ampoule was quenched in ice water to preclude possible structural phase transitions at intermediate temperatures.

B. Single crystal X-ray diffraction

Room temperature single-crystal X-ray diffraction data [see Fig. 1(a)] were collected on a single crystal fragment of $\text{Fe}_{0.67}\text{Cr}_2\text{Te}_4$ mounted on glass fibers with two-part epoxy

using a Bruker Kappa D8 Quest diffractometer with an $I\mu\text{S}$ microfocus source (Mo K_α radiation, $\lambda = 0.71073 \text{ \AA}$), PHOTON III CPAD detector, and a HELIOS optics monochromator. Integration was performed using the Bruker SAINT program, and absorption correction was done using the SADABS 2016/2 program [22]. SHELXL was used to anisotropically refine the preliminary model obtained from SHELXT by intrinsic phasing [23,24]. Preliminary indexing of diffraction reflections led to a hexagonal unit cell closely related to the NiAs structure-type, but after considering systematic absence violations, a better model was found using the trigonal $P\bar{3}m1$ space group. Due to the nature of X-ray diffraction, the similar structure factors of Fe and Cr make it difficult to quantify the amount of site mixing and would require further investigations via other techniques, such as neutron diffraction. The Wyckoff site $1a$ was modeled as a fully occupied Cr transition metal layer, with the Wyckoff site $1b$ modeled as a partially occupied Fe transition metal (TM) layer. This modeling is in line with the literature [25]. The model was allowed to refine freely, without constraints to fit the EDS data, and similar compositions of Fe and Cr were obtained between both techniques. Therefore, $\text{Fe}_x\text{Cr}_2\text{Te}_4$ could be grown in 2 distinct crystallographic phases, $I2/m$ and $P\bar{3}m1$, although $\text{Fe}_{2/3}\text{Cr}_2\text{Te}_4$ has a distinct stoichiometry with respect to FeCr_2Te_4 , i.e., with the nominal composition FeCr_3Te_6 .

Refinement of the lattice parameters of FeCr_3Te_6 yields $a = 3.9313(7) \text{ \AA}$, and $c = 5.9158(16) \text{ \AA}$, for a $V = 79.18(4) \text{ \AA}^3$. The bulk crystallographic structure of FeCr_3Te_6 is illustrated in Fig. 1(b). For additional discussion, as well as the crystallographic data, atomic coordinates, and atomic displacement parameters, see the Supplemental Material [26] and Refs. [27–36] therein.

C. Electronic band structure calculations

First-principles density functional theory (DFT) calculations were performed using the projector augmented-wave (PAW) potentials [37] implemented in the Vienna *Ab-initio* Simulation Package (VASP) [38–40].

For the exchange-correlation energy, the generalized gradient approximation (GGA) in the Perdew–Burke–Ernzerhof (PBE) parametrization was used [41]. The energy cutoff for the plane-wave expansion was set to 400 eV. Optimization of the lattice constants and atomic positions was performed

in the presence of spin-orbit coupling (SOC). The structure was optimized using a $10 \times 10 \times 5$ \mathbf{k} -point Monkhorst–Pack grid [42]. As for the convergence criterion of the optimization loop, we chose an energy change inferior to 10^{-6} eV and 10^{-8} eV for the ionic and electronic degrees of freedom, respectively.

The symmetry of the structures after optimization was analyzed with FINDSYM [43] and SPGLIB [44], while the momentum space analysis was performed within SEEK-PATH [45].

Motivated by a previous study on CrTe_2 [46], we chose to apply the DFT+ U scheme. The U parameter for the DFT+ U treatment of Cr d -electrons in CrTe_2 within the linear response ansatz of Cococcioni *et al.* [47] can be expressed as:

$$U_{\text{eff}} = \frac{1}{\chi} - \frac{1}{\chi_0}, \quad (1)$$

where $\chi \approx \partial N^{\text{SCF}}/\partial U$ and $\chi_0 \approx \partial N^{\text{NSCF}}/\partial U$ correspond to the self-consistent (SCF) and non-self-consistent (NSCF) response function. These calculations were performed within a supercell $2 \times 2 \times 2$ and reduced to a $6 \times 6 \times 3\Gamma$ -centered \mathbf{k} -grid. From the DFT calculations we found $\chi \approx 0.17 \text{ eV}^{-1}$ and $\chi_0 \approx 0.81 \text{ eV}^{-1}$, which corresponds to an effective U of ~ 4.5 eV. However, the lattice parameters were found to depend strongly on U (see Fig. S2 in the SM [26]). Thus, we apply the DFT + U approach introduced by Dudarev *et al.* [48], with $U \approx 4$ eV, which is closer to the linear response interpolated value.

After optimization of the clean system, we obtain $a = b = 4.00 \text{ \AA}$ and $c = 6.14 \text{ \AA}$, which are relatively close to the experimental values $a = b \simeq 3.93 \text{ \AA}$ and $c \simeq 5.92 \text{ \AA}$ [49]. Atomic sites at high symmetry Wyckoff positions are Cr $1a$ (0,0,0) and Te $2d$ ($1/3, 2/3, z_{\text{Te}}$), where the free parameter converged to $z_{\text{Te}} = 0.250$.

Magnetic order—Cr-Te compounds typically are ferromagnets with out-of-the-plane magnetic moments [50–52], with strong magnetic anisotropy [53,54]. The magnetic ground state was found to display $M \parallel c$, which is in agreement with a previous study in CrTe_2 [55] and, as we will see below, with the fact that the c -axis is the magnetic easy axis for FeCr_3Te_6 .

The resulting electronic band structure both with (blue lines) and without (orange lines) spin-orbit coupling (SOC) is shown in Fig. 2. Salient features are the nearly linear and tilted crossings (indicated by magenta circles) along the M- Γ , A-H, and L-A directions, with the first crossing occurring precisely at the Fermi level. These crossings at or very close to ε_F , classified as type-II Dirac nodes, ought to become type-II Weyl nodes [56,57], once the system breaks time-reversal symmetry upon entering its ferromagnetic ground-state, as will be discussed below. Another feature is the presence of a rather flat band along the M-A direction that crosses ε_F . Therefore, FeCr_3Te_6 presents a certain similarity with kagome systems, which exhibit the coexistence between flat and linearly dispersing bands [58]. The flat bands in kagomes are said to become topological in character due to spin-orbit coupling [58] under broken time-reversal symmetry, leading, in certain compounds, to a large intrinsic anomalous Hall response [59]. Under these conditions, the flat bands could acquire

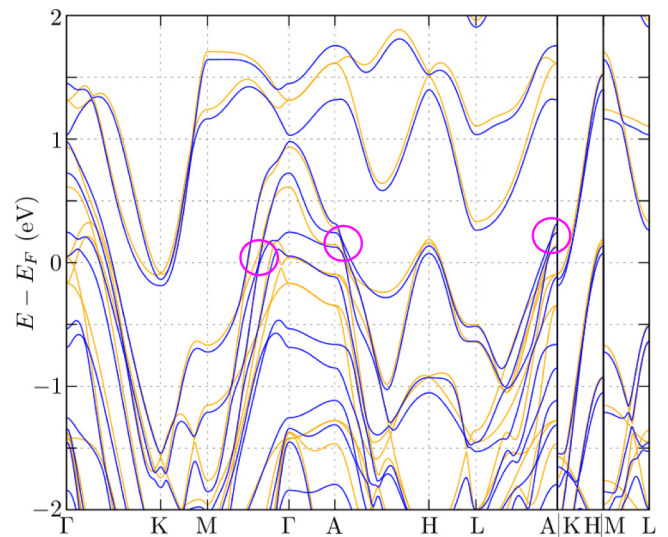


FIG. 2. The electronic band structures for well-ordered FeCr_3Te_6 . Results in the absence and presence of the spin-orbit coupling (orange and blue lines, respectively).

a nonzero Chern number associated with a nontrivial Berry phase that would support interacting topological phases [60]. The experimental confirmation of the calculated electronic band structure, for example, to expose the presence of flat bands and Dirac/Weyl dispersions would require measurements of quantum oscillatory phenomena, or angle-resolved photoemission spectroscopy experiments (ARPES). Current levels of disorder in our crystals preclude the observation of quantum oscillations. ARPES measurements will have to be performed in collaborative mode; therefore, these will be left for a future report.

Here, the fundamental question is whether the coexistence between type-II Weyl fermions and flat bands intersecting the Fermi level in FeCr_3Te_6 , which are subjected to spin-orbit interaction, would lead to a very large anomalous Hall response under broken time-reversal symmetry. As for the kagome compounds, this would point to nontrivial band topology. To address this question, we performed detailed transport and magnetization measurements as a function of temperature and magnetic field. Notice that the calculations above assume an ordered FeCr_3Te_6 structure, when in reality, single-crystal X-ray diffraction points to a random occupation of the Fe site. Such disorder and associated scattering are likely to affect the transport properties of this compound.

D. Magnetization measurements

DC magnetization (M) measurements were performed in a superconducting quantum interference device-based magnetometer (Quantum Design MPMS-XL). We studied the magnetization of FeCr_3Te_6 single-crystals as a function of temperature T for T ranging from 1.8 K to 300 K under external magnetic fields $-7 \text{ T} \leq \mu_0 H \leq 7 \text{ T}$. M as a function of T was collected using the zero-field-cooled (ZFC) and field-cooled (FC under $\mu_0 H = 300 \text{ Oe}$) protocols.

Figures 3(a) and 3(b) show M as a function of T when an external field $\mu_0 H = 300 \text{ Oe}$ is applied along either the

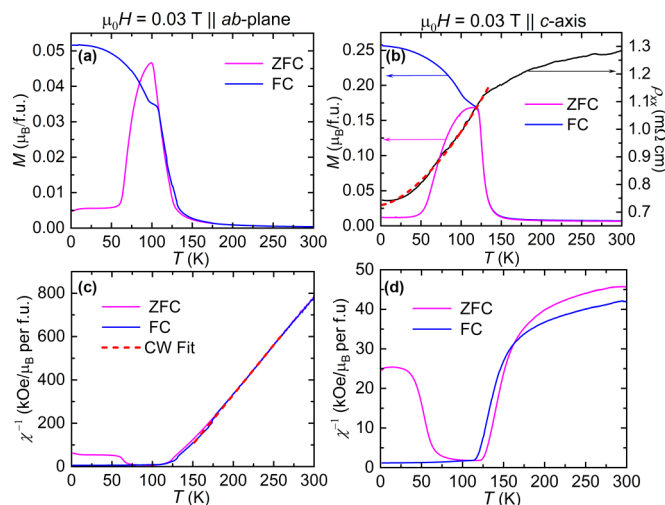


FIG. 3. (a) Magnetization M (in μ_B per f.u.) collected under a magnetic field ($\mu_0 H = 300$ Oe) applied along the ab -plane of the crystal as a function of temperature T . Magenta circles and blue lines correspond to zero-field-cooled (ZFC) and field-cooled (FC) conditions, respectively. (b) Magnetization M for fields aligned along the c -axis of the crystal. This panel also includes the in-plane resistivity ρ_{xx} (black trace) as a function of T . Dashed red line is a fit to a Fermi liquid like, T^2 dependence for the resistivity at low temperatures. (c) Inverse magnetic susceptibility χ^{-1} as a function of T . The red dashed line is a linear or Curie-Weiss fit. (d) χ^{-1} as a function of T for fields along the c -axis. See Fig. S4 [26] for M as a function of T from a second crystal also displaying a two-step transition.

ab -plane or the c -axis of the crystal, respectively. For both orientations, we found a two-step ferromagnetic transition below $T_c \simeq 120$ K. The values of M for fields applied along the c -axis are larger than those collected under fields applied along the ab -plane, reflecting the magneto-crystalline anisotropy of FeCr_3Te_6 . Figures 3(c) and 3(d) plot the inverse magnetic susceptibility $\chi^{-1}(T)$ as a function of T for both field orientations. A Curie-Weiss fit [Fig. 3(c)] is used to extract the effective magnetic moment yielding $\mu_{\text{eff}} = 1.34 \mu_B$ per formula unit when the external field is applied along the ab -plane. For reasons that remain unclear to us, we cannot observe a clear Curie-Weiss behavior for $\mu_0 H \parallel c$ -axis.

To more clearly expose the existence of two ferromagnetic transitions upon cooling, we took the derivative of the DC magnetization M with respect to T under field-cooling conditions (see Fig. 4). As seen in both Figs. 3 and 4, the

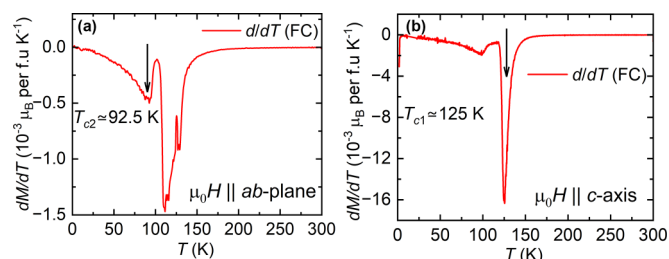


FIG. 4. Derivative of the magnetization M with respect to temperature T collected under field-cooling conditions, for fields applied along (a) the ab -plane and (b) the c -axis of the crystal.

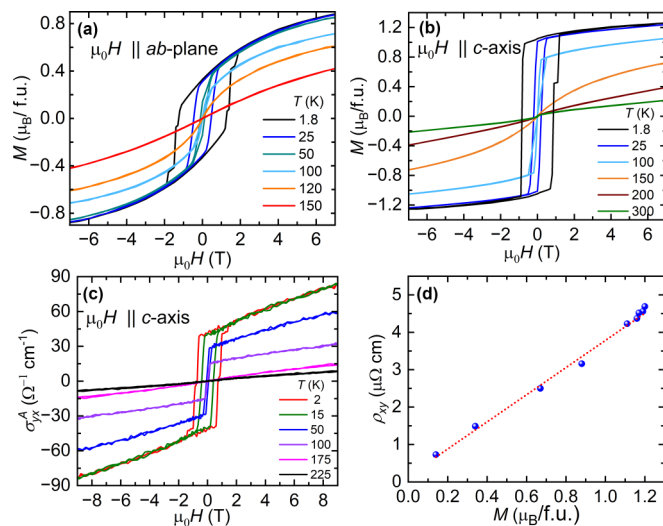


FIG. 5. DC magnetization M (in μ_B per f.u.) as a function of the magnetic field $\mu_0 H$ for several temperatures with the field oriented along (a) the ab -plane and (b) the c -axis, respectively. (c) Anomalous Hall conductivity as a function of the magnetic field at various T s, with $\mu_0 H$ applied along the c -axis of the crystal. (d) Dependence of the anomalous Hall resistivity as a function of M .

ferromagnetic transition at higher temperatures is sharper for $\mu_0 H \parallel c$ -axis, while the lower T one is slightly sharper for fields along the ab -plane. $\partial M/\partial T$ yields two transition temperatures, whose middle transition points are $T_{c1} \simeq 125$ K and $T_{c2} \simeq 92.5$ K. At first glance, the existence of two Curie temperatures would suggest two magnetic sub-lattices ordering at distinct temperatures. Neutron-scattering measurements will be required to clarify the origin of both Curie temperatures.

M as a function of the magnetic field orientation for several T s is shown in Figs. 5(a) and 5(b) for $\mu_0 H$ ranging from -7 T to 7 T. Notice that lower fields are required to saturate M for fields along the c -axis with respect to fields applied along the ab -plane. Furthermore, at the lowest T s, under $\mu_0 H = 7$ T, M becomes nearly saturated, reaching a value of $1.2 \mu_B$ per formula unit (f.u.), which is nearly $\sim 50\%$ higher than the value observed for fields along the ab -plane under the same field and temperature conditions. This means that the c -axis is the magnetization easy axis and FeCr_3Te_6 presents a mild magneto-crystalline anisotropy.

At the lowest $T = 1.8$ K, we extracted slightly larger coercive fields $\mu_0 H_c^{\text{ab}} \simeq 1.3$ T for fields along the ab -plane relative to fields along the c -axis, i.e., $\mu_0 H_c^c \simeq 0.85$ T. For both field orientations, we observe small steps around the coercive field associated with ferromagnetic domain reorientation.

E. Electrical transport measurements

Subsequently, we proceeded with measurements of the Hall resistivity ρ_{xy} , as well as magneto-resistivity ρ_{xx} collected in a Physical Property Measurement System (PPMS) from Quantum Design. Single crystals were locally etched via Ar ions to remove a possible oxidation layer. Subsequently, a layer of Au was deposited via magnetron sputtering to improve the electrical contacts. Platinum wires, with a diameter $\phi = 25 \mu\text{m}$, were attached to these contacts with silver paint.

Resistivity as a function of the temperature was measured for T ranging from 300 K to 1.8 K. Hexagonal-shaped crystals were used for these measurements with the magnetic field applied along the c -axis. To eliminate the contribution of ρ_{xx} into ρ_{xy} due to contact misalignment, or of ρ_{xy} into ρ_{xx} , we anti-symmetrized the $\rho_{xy}(\mu_0 H)$ traces for both field orientations and averaged the $\rho_{xx}(\mu_0 H)$ ones collected at each T .

The resistivity ρ_{xx} as a function of the T is also shown in Fig. 3(b). $\rho_{xx}(T)$ exhibits metallic behavior with a change in its slope near $T_c \sim 125$ K associated with the paramagnetic (PM) to ferromagnetic (FM) transition. This sample yields a residual resistivity ratio (RRR = $\rho(300 \text{ K})/\rho(1.8 \text{ K})$) of ~ 1.84 . This small value, when combined with the large residual resistivity of $750 \mu\Omega \text{ cm}$, suggests that the electrical transport in this compound is dominated by the disorder inherent in the Fe distribution in the compound.

The Hall conductivity $\sigma_{xy} = \rho_{xy}/(\rho_{xx}^2 + \rho_{yy}^2)$, where ρ_{xy} is the Hall resistivity, is shown in Fig. 5(c) for fields oriented along the c -axis of the crystal and for several T s. σ_{xy} mimics the behavior of M shown in Fig. 5(b), indicating a pronounced anomalous Hall component. The maximum value attained by σ_{xy} is $40.68 \Omega^{-1} \text{ cm}^{-1}$ at 2 K under $\mu_0 H \simeq 1$ T (which is considerably smaller than $\sim 823 \Omega^{-1} \text{ cm}^{-1}$ for thin Fe films [61] at room T) decreases as the temperature increases. Such modest values for σ_{xy} suggest that the anomalous Hall is not dominated by the intrinsic but rather the extrinsic scattering-dominated contribution [8]. Similarly to the magnetization [Fig. 5(b)], σ_{xy} displays coercive fields below $T \simeq 75$ K. We confirmed that the Hall signal is proportional to the magnetization of the crystal, as expected for the anomalous Hall response. Figure 5(d) shows that the value of $\rho_{xy}(\mu_0 H = 2 \text{ T})$ just above the coercive fields scales linearly with M . The coercive fields are also evident in the magnetoresistivity of FeCr_3Te_6 , which decreases as the temperature increases (see SM [26]).

As previously mentioned, and as discussed in Ref. [8], the anomalous Hall signal originates from both intrinsic and extrinsic contributions. The intrinsic contribution results from the deflection of the trajectory of the charge carriers due to the Berry curvature in momentum space [7], which is intrinsic to the electronic bands of a given compound. The extrinsic contributions are provided by the skew, or asymmetric scattering, and by side jumps in the presence of spin-orbit coupling and impurities. We followed the scaling analysis of the Hall signal, as proposed by Ref. [61], to evaluate the relative strengths of the intrinsic and extrinsic contributions. In Fig. 6(a), the anomalous Hall resistivity is plotted as a function of the square of the magnetoresistivity:

$$\sigma_{xy}^A = \frac{\rho_{xy}^A}{(\rho_{xy}^A)^2 + \rho_{xx}^2} = -(\alpha\sigma_{xx0}^{-1} + \beta\sigma_{xx0}^{-2})\sigma_{xx}^2 - b. \quad (2)$$

Here, $\rho_{xy}^A = \rho_{xy}(\mu_0 H = 2 \text{ T})$, since the Hall signal becomes saturated at this field value, although it is dominated by a linear component inherent to the conventional Hall response. According to Ref. [61], the intercept would yield the size of the intrinsic contribution, with the slope providing the magnitude of the extrinsic one.

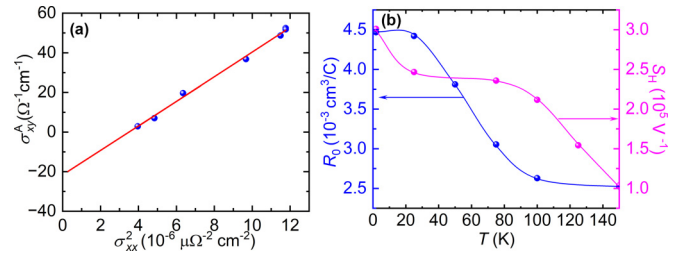


FIG. 6. (a) Anomalous Hall conductivity σ_{xy}^A as a function of the square of the magnetoconductivity σ_{xx}^2 . (b) Conventional Hall constant R_0 (blue markers) and anomalous Hall coefficient S_H (magenta markers) as functions of the temperature.

A linear fit yields a slope of $6.23 \Omega \text{ cm}$ and an intercept of $\sim 21.9 (\Omega \text{ cm})^{-1}$. Therefore, the anomalous Hall effect of FeCr_3Te_6 has a sizable intrinsic contribution, as implied by the calculations, although with a large superimposed extrinsic contribution due to disorder. To place the value of the intercept in perspective, thin films of Fe yielded $\sim 1100 (\Omega \text{ cm})^{-1}$ [61].

It has been assumed by the scientific community—and recently shown theoretically [7]—that the Hall response of magnetic compounds, in particular those displaying noncoplanar spin textures, can be treated as the summation of three contributions:

$$\rho_{xy} = \rho_{xy}^N + \rho_{xy}^A + \rho_{xy}^T, \quad (3)$$

$$\rho_{xy} = R_0 B + S_H M \rho_{xx}^2 + \rho_{xy}^T. \quad (4)$$

The first term corresponds to the conventional Hall effect, with R_0 being the Hall coefficient; the second term ρ_{xy}^A corresponds to the anomalous Hall contribution which, as shown in Fig. 5(d), scales linearly with M , and, as shown in Fig. 6(a), also with $\rho_{xx}^2 \simeq \sigma_{xx}^{-2}$. S_H is the proportionality constant between these physical variables. Figure 6(b) displays both R_0 and S_H as functions of T , with R_0 increasing upon cooling, suggesting an increase in carrier mobilities. In contrast S_H emerges below T_c and remains nearly constant below $T = 100$ K.

The topological Hall contribution to the Hall response [7] can be extracted from Eq. (3) by subtracting both the conventional and anomalous Hall contributions. Such a subtraction requires a precise determination of S_H , or a plot of ρ_{xy} as a function of $M\rho_{xx}^2$ [see Fig. 7(a)], to confirm their linear relation. From this plot, S_H is extracted from a simple linear fit. Once S_H is determined, one can subtract the anomalous Hall component from the raw ρ_{xy} . Figure 7(b) displays the remnant of this subtraction, or the topological Hall signal ρ_{xy}^T (in addition to a small conventional Hall component) from FeCr_3Te_6 for $\mu_0 H \parallel c$ -axis and for different temperatures. Below $T = 25$ K, one observes the sudden emergence of a peak displaying a maximum $\leq 1 \mu\Omega \text{ cm}$, whose position is displaced from $\mu_0 H^p \simeq 0.3 \text{ T}$ at $T = 25 \text{ K}$ to $\mu_0 H^p \simeq 1.0 \text{ T}$ at $T = 5 \text{ K}$. ρ_{xy}^T displays a complex structure at $T = 1.8 \text{ K}$, likely resulting from contamination by the large hysteresis observed in both magnetization and Hall response at this temperature. Notice that these peaks are reproducible among different crystals; see Fig. S5 [26], which displays ρ_{xy}^T for a second

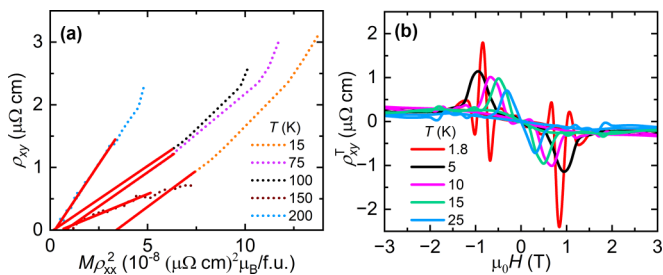


FIG. 7. (a) Anomalous Hall resistivity ρ_{xy} as a function of the product of the magnetization by the square of the magnetoresistivity. Red lines are linear fits from which we extract the values of S_H . (b) Topological Hall signal for FeCr_3Te_6 for fields $\mu_0 H \parallel c$ -axis and for different T s after subtracting $S_H M \rho_{xx}^2$ from the raw ρ_{xy} .

crystal whose ρ_{xy}^T peaks display considerably larger amplitudes, i.e., surpassing $2 \mu\Omega \text{ cm}$.

The presence of chiral spin textures and a concomitant topological Hall signal is usually associated with the absence of inversion symmetry, or the presence of the Dzyaloshinskii–Moriya interaction in ferromagnetic systems [62]. Notice that our X-ray diffraction refinement yields the $P\bar{3}m1$ space group for FeCr_3Te_6 , which, by contrast, is centrosymmetric. Here, the situation seems to be akin to those of the $\text{Fe}_{3-x}\text{GeTe}_2$ and Fe_3GaTe_2 compounds, which were reported to crystallize in the centrosymmetric $P6_3/mmc$ space group [63,64], while still displaying skyrmions [65–68]. It was proposed that Fe vacancy order might contribute to locally breaking the inversion symmetry contributing to the stabilization of skyrmions in, for instance, $\text{Fe}_{3-x}\text{GeTe}_2$ [69].

In FeCr_3Te_6 the presence of chiral spin textures at relatively high magnetic fields will have to be confirmed via imaging techniques like magnetic force microscopy. If confirmed, one would still have to understand the physical mechanism(s) leading to their formation.

III. CONCLUSIONS

In conclusion, we explored the structural, electrical transport and magnetic properties of a new crystallographic phase within the Cr-Fe-Te series, namely ferromagnetic $\text{Fe}_{1/3}\text{CrTe}_2$, which can be grown in single-crystalline form. According to electronic band structure calculations, FeCr_3Te_6 displays type-II Dirac nodes along with electronic flat bands near or at the Fermi level. This makes FeCr_3Te_6 a good candidate for novel transport properties, such as a large anomalous Hall

response. FeCr_3Te_6 displays a pronounced anomalous Hall effect below the Curie temperature $T_c = 120 \text{ K}$, which is characterized by a significant intrinsic contribution dominated by the Berry phase, according to a scaling analysis, and as expected from the calculations. A sizable extrinsic contribution is also superimposed on the anomalous Hall response according to the same scaling analysis. Therefore, we conclude that the transport properties of FeCr_3Te_6 are also affected by the occupational disorder at the 1b Fe-site within the van der Waals gap of the CrTe_2 host.

Upon cooling, FeCr_3Te_6 displays a second ferromagnetic transition at $T_{c2} \sim 92.5 \text{ K}$. By further cooling this compound, we observe the emergence of a clear topological Hall signal below $T = 25 \text{ K}$, pointing to the possible presence of chiral spin textures, such as skyrmions. This signal is reproducible among several crystals. However, their presence would be inconsistent with the inversion symmetry inherent in the refined structure of FeCr_3Te_6 . Advanced imaging techniques, such as Lorentz transmission electron microscopy (unlikely given the low temperatures and high magnetic fields required for their observation) and magnetic force microscopy, will be required to expose their presence [70]. If their presence were confirmed, an intriguing aspect to be studied would be their evolution as a function of field and temperature, given that at liquid helium temperatures, the topological Hall effect peaks at fields as large as $\mu_0 H = 1 \text{ T}$, indicating a particular resilience with respect to field application. One would also need to understand the mechanism(s) leading to skyrmion formation in this compound.

ACKNOWLEDGMENTS

L.B. acknowledges support from the U.S. Department of Energy, Basic Energy Sciences (BES) program through Award No. DE-SC0002613. J.Y.C. acknowledges the U.S. Department of Energy Basic Award No. DE-SC0022854 and the Welch Foundation through Award No. AA-2056-20240404. The National High Magnetic Field Laboratory acknowledges support from the U.S. National Science Foundation (NSF) Cooperative agreement, Grant No. DMR-2128556, and the state of Florida.

DATA AVAILABILITY

The data that support the findings in this article were uploaded onto the Open Source Framework website [71] and can be accessed through [72].

- [1] J. M. D. Coey, Hard magnetic materials: A perspective, *IEEE Trans. Magn.* **47**, 4671 (2011).
- [2] J. Cui, M. Kramer, L. Zhou, F. Liu, A. Gabay, G. Hadjipanayis, B. Balasubramanian, and D. Sellmyer, Current progress and future challenges in rare-earth-free permanent magnets, *Acta Mater.* **158**, 118 (2018).
- [3] B. A. Bernevig, C. Felser, and H. Beidenkopf, Progress and prospects in magnetic topological materials, *Nature (London)* **603**, 41 (2022).

- [4] F. D. M. Haldane, Model for a quantum Hall effect without Landau levels: Condensed-matter realization of the “parity anomaly”, *Phys. Rev. Lett.* **61**, 2015 (1988).
- [5] C.-Z. Chang, J. Zhang, X. Feng, J. Shen, Z. Zhang, M. Guo, K. Li, Y. Ou, P. Wei, L.-L. Wang, Z.-Q. Ji, Y. Feng, S. Ji, X. Chen, J. Jia, X. Dai, Z. Fang, S.-C. Zhang, K. He, Y. Wang *et al.*, Experimental observation of the quantum anomalous Hall effect in a magnetic topological insulator, *Science* **340**, 167 (2013).

- [6] E. M. Pugh and N. Rostoker, Hall effect in ferromagnetic materials, *Rev. Mod. Phys.* **25**, 151 (1953).
- [7] N. Verma, Z. Addison, and M. Randeria, Unified theory of the anomalous and topological Hall effects with phase-space Berry curvatures, *Sci. Adv.* **8**, eabq2765 (2022).
- [8] N. Nagaosa, J. Sinova, S. Onoda, A. H. MacDonald, and N. P. Ong, Anomalous Hall effect, *Rev. Mod. Phys.* **82**, 1539 (2010).
- [9] R. Karplus and J. M. Luttinger, Hall effect in ferromagnetics, *Phys. Rev.* **95**, 1154 (1954).
- [10] T. Jungwirth, Q. Niu, and A. H. MacDonald, Anomalous Hall effect in ferromagnetic semiconductors, *Phys. Rev. Lett.* **88**, 207208 (2002).
- [11] M. Onoda and N. Nagaosa, Quantized anomalous Hall effect in two-dimensional ferromagnets: Quantum Hall effect in metals, *Phys. Rev. Lett.* **90**, 206601 (2003).
- [12] L. Berger, Side-jump mechanism for the Hall effect of ferromagnets, *Phys. Rev. B* **2**, 4559 (1970).
- [13] J. Smit, The spontaneous Hall effect in ferromagnetics I, *Physica* **21**, 877 (1955).
- [14] J. Smit, The spontaneous Hall effect in ferromagnetics II, *Physica* **24**, 39 (1958).
- [15] J. Bertinshaw, C. Ulrich, A. Guenther, F. Schrettle, M. Wohlaue, S. Krohns, M. Reehuis, A. J. Studer, M. Avdeev, D. V. Quach, J. R. Groza, V. Tsurkan, A. Loidl, and J. Deisenhofer, FeCr_2S_4 in magnetic fields: Possible evidence for a multiferroic ground state, *Sci. Rep.* **4**, 6079 (2014).
- [16] Y. Liu, R. J. Koch, Z. Hu, N. Aryal, E. Stavitski, X. Tong, K. Attenkofer, E. S. Bozin, W. Yin, and C. Petrovic, Three-dimensional Ising ferrimagnetism of Cr-Fe-Cr trimers in FeCr_2Te_4 , *Phys. Rev. B* **102**, 085158 (2020).
- [17] V. Tsurkan, O. Zaharko, F. Schrettle, C. Kant, J. Deisenhofer, H.-A. Krug von Nidda, V. Felea, P. Lemmens, J. R. Groza, D. V. Quach, F. Gozzo, and A. Loidl, Structural anomalies and the orbital ground state in FeCr_2S_4 , *Phys. Rev. B* **81**, 184426 (2010).
- [18] A. Ramirez, R. Cava, and J. Krajewski, Colossal magnetoresistance in Cr-based chalcogenide spinels, *Nature (London)* **386**, 156 (1997).
- [19] B. I. Min, S. S. Baik, H. C. Choi, S. K. Kwon, and J.-S. Kang, Electronic structures of magnetic semiconductors FeCr_2Se_4 and $\text{Fe}_{0.5}\text{Cu}_{0.5}\text{Cr}_2\text{Se}_4$, *New J. Phys.* **10**, 055014 (2008).
- [20] G. J. Snyder, T. Caillat, and J.-P. Fleurial, Thermoelectric transport, and magnetic properties of the polaron semiconductor $\text{Fe}_x\text{Cr}_{3-x}\text{Se}_4$, *Phys. Rev. B* **62**, 10185 (2000).
- [21] Y. Liu, H. Tan, Z. Hu, B. Yan, and C. Petrovic, Anomalous Hall effect in the weak-itinerant ferrimagnet FeCr_2Te_4 , *Phys. Rev. B* **103**, 045106 (2021).
- [22] L. Krause, R. Herbst-Irmer, G. M. Sheldrick, and D. Stalke, Comparison of silver and molybdenum microfocus X-ray sources for single-crystal structure determination, *J. Appl. Crystallogr.* **48**, 3 (2015).
- [23] G. M. Sheldrick, Crystal structure refinement with SHELXL, *Acta Crystallographica Section C* **71**, 3 (2015).
- [24] G. M. Sheldrick, *SHELXT*—Integrated space-group and crystal-structure determination, *Acta Crystallogr. Sect. A* **71**, 3 (2015).
- [25] J.-Q. Yan, B. Saparov, A. S. Sefat, H. Yang, H. B. Cao, H. D. Zhou, B. C. Sales, and D. G. Mandrus, Absence of structural transition in $M_{0.5}\text{IrTe}_2$ ($M = \text{Mn, Fe, Co, Ni}$), *Phys. Rev. B* **88**, 134502 (2013).
- [26] See Supplemental Material at <http://link.aps.org/supplemental/10.1103/PhysRevMaterials.9.044203> for detailed crystal structure analysis of FeCr_3Te_6 , calculated lattice constants as a function of the correlation strength U , magnetoresistivity of FeCr_3Te_6 as function of the magnetic field (μ_0H) and temperature (T), reproducibility of both the topological Hall response and double ferromagnetic transitions among different FeCr_3Te_6 crystals, magnetization M collected under μ_0H applied along the c -axis for a second FeCr_3Te_6 crystal as a function of T , derivative of M with respect to T exposing both ferromagnetic transitions, analysis of the anomalous and topological Hall responses, and topological Hall signal for a second FeCr_3Te_6 crystal.
- [27] J. Yang, C. Zhu, Y. Deng, B. Tang, and Z. Liu, Magnetism of two-dimensional chromium tellurides, *iScience* **26**, 106567 (2023).
- [28] Z.-L. Huang, W. Bensch, D. Benea, and H. Ebert, Anion substitution effects on structure and magnetism in the chromium chalcogenide Cr_5Te_8 —Part I: Cluster glass behavior in trigonal $\text{Cr}_{(1+x)}\text{Q}_2$ with basic cell ($\text{Q} = \text{Te, Se}$; $\text{Te:Se} = 7:1$), *J. Solid State Chem.* **177**, 3245 (2004).
- [29] Z.-L. Huang, W. Bensch, S. Mankovsky, S. Polesya, H. Ebert, and R. K. Kremer, Anion substitution effects on structure and magnetism of the chromium chalcogenide Cr_5Te_8 —Part II: Cluster-glass and spin-glass behavior in trigonal $\text{Cr}_{(1+x)}\text{Q}_2$ with basic cells and trigonal $\text{Cr}_{(5+x)}\text{Q}_8$ with superstructures ($\text{Q} = \text{Te, Se}$; $\text{Te:Se} = 6:2$), *J. Solid State Chem.* **179**, 2067 (2006).
- [30] M. Chevreton, E. F. Bertaut, and F. Jelinek, Quelques remarques sur le système Cr—Te, *Acta Crystallogr.* **16**, 431 (1963).
- [31] A. F. Andresen, A neutron diffraction investigation of Cr_2Te_3 and Cr_5Te_6 , *Acta Chem. Scand.* **17**, 1335 (1963).
- [32] A. Williams and J. Goldberger, The zoology of two-dimensional van der Waals materials, in *Comprehensive Inorganic Chemistry III (Third Edition)*, edited by J. Reedijk and K. R. Poeppelmeier (Elsevier, Oxford, 2023), pp. 449–498.
- [33] Y. Hinatsu, T. Tsuji, and K. Ishida, Magnetic properties of $(\text{Cr}_{1-x}\text{Fe}_x)_3\text{Te}_4$, *J. Solid State Chem.* **120**, 49 (1995).
- [34] R. H. Plovnick, Preparation and properties of iron vanadium telluride, FeV_2Te_4 , *J. Solid State Chem.* **5**, 153 (1972).
- [35] K. Yasui, K. Ishida, and T. Tsuji, Heat capacity measurement of $(\text{Cr}_{1-x}\text{Fe}_x)_3\text{Te}_4$ ($x = 0 - 0.1$) at high temperatures, *J. Nucl. Mater.* **247**, 345 (1997).
- [36] S. Routh, I. Kar, A. Low, S. Ghosh, and T. K. Bhowmik, Magnetoresistance behavior across the critical region in ferrimagnet FeCr_2Te_4 single crystal, *Phys. Lett. A* **486**, 129101 (2023).
- [37] P. E. Blöchl, Projector augmented-wave method, *Phys. Rev. B* **50**, 17953 (1994).
- [38] G. Kresse and J. Hafner, *Ab initio* molecular-dynamics simulation of the liquid-metal–amorphous-semiconductor transition in germanium, *Phys. Rev. B* **49**, 14251 (1994).
- [39] G. Kresse and J. Furthmüller, Efficient iterative schemes for *ab initio* total-energy calculations using a plane-wave basis set, *Phys. Rev. B* **54**, 11169 (1996).
- [40] G. Kresse and D. Joubert, From ultrasoft pseudopotentials to the projector augmented-wave method, *Phys. Rev. B* **59**, 1758 (1999).
- [41] J. P. Perdew, K. Burke, and M. Ernzerhof, Generalized gradient approximation made simple, *Phys. Rev. Lett.* **77**, 3865 (1996).
- [42] H. J. Monkhorst and J. D. Pack, Special points for Brillouin-zone integrations, *Phys. Rev. B* **13**, 5188 (1976).

- [43] H. T. Stokes and D. M. Hatch, FINDSYM: program for identifying the space-group symmetry of a crystal, *J. Appl. Cryst.* **38**, 237 (2005).
- [44] K. S. Atsushi Togo and I. Tanaka, Spglib: A software library for crystal symmetry search, *Sci. Technol. Adv. Mater.* **4**, 2384822 (2024).
- [45] Y. Hinuma, G. Pizzi, Y. Kumagai, F. Oba, and I. Tanaka, Band structure diagram paths based on crystallography, *Comput. Mater. Sci.* **128**, 140 (2017).
- [46] Y. Liu, S. Kwon, G. J. de Coster, R. K. Lake, and M. R. Neupane, Structural, electronic, and magnetic properties of CrTe₂, *Phys. Rev. Mater.* **6**, 084004 (2022).
- [47] M. Cococcioni and S. de Gironcoli, Linear response approach to the calculation of the effective interaction parameters in the LDA + U method, *Phys. Rev. B* **71**, 035105 (2005).
- [48] S. L. Dudarev, G. A. Botton, S. Y. Savrasov, C. J. Humphreys, and A. P. Sutton, Electron-energy-loss spectra and the structural stability of nickel oxide: An LSDA + U study, *Phys. Rev. B* **57**, 1505 (1998).
- [49] L. Meng, Z. Zhou, M. Xu, S. Yang, K. Si, L. Liu, X. Wang, H. Jiang, B. Li, P. Qin, P. Zhang, J. Wang, Z. Liu, P. Tang, Y. Ye, W. Zhou, L. Bao, H.-J. Gao, and Y. Gong, Anomalous thickness dependence of Curie temperature in air-stable two-dimensional ferromagnetic 1T-CrTe₂ grown by chemical vapor deposition, *Nat. Commun.* **12**, 809 (2021).
- [50] X. Sun, W. Li, X. Wang, Q. Sui, T. Zhang, Z. Wang, L. Liu, D. Li, S. Feng, S. Zhong, H. Wang, V. Bouchiat, M. Nunez Regueiro, N. Rougemaille, J. Coraux, A. Purbawati, A. Hadj-Azzem, Z. Wang, B. Dong, X. Wu *et al.*, Room temperature ferromagnetism in ultra-thin van der Waals crystals of 1T-CrTe₂, *Nano Res.* **13**, 3358 (2020).
- [51] Y. Wen, Z. Liu, Y. Zhang, C. Xia, B. Zhai, X. Zhang, G. Zhai, C. Shen, P. He, R. Cheng, L. Yin, Y. Yao, M. Getaye Sendeku, Z. Wang, X. Ye, C. Liu, C. Jiang, C. Shan, Y. Long, and J. He, Tunable room-temperature ferromagnetism in two-dimensional Cr₂Te₃, *Nano Lett.* **20**, 3130 (2020).
- [52] X. Zhang, Q. Lu, W. Liu, W. Niu, J. Sun, J. Cook, M. Vaninger, P. F. Miceli, D. J. Singh, S.-W. Lian, T.-R. Chang, X. He, J. Du, L. He, R. Zhang, G. Bian, and Y. Xu, Room-temperature intrinsic ferromagnetism in epitaxial CrTe₂ ultrathin films, *Nat. Commun.* **12**, 2492 (2021).
- [53] T. Hirone and S. Chiba, On the magnetic anisotropy of single crystal of chromium telluride, *J. Phys. Soc. Jpn.* **15**, 1991 (1960).
- [54] M. G. Sreenivasan, K. L. Teo, X. Z. Cheng, M. B. A. Jalil, T. Liew, T. C. Chong, A. Y. Du, T. K. Chan, and T. Osipowicz, Structural, magnetic, and transport investigations of CrTe clustering effect in (Zn,Cr)Te system, *J. Appl. Phys.* **102**, 053702 (2007).
- [55] Y. Fujisawa, M. Pardo-Almanza, J. Garland, K. Yamagami, X. Zhu, X. Chen, K. Araki, T. Takeda, M. Kobayashi, Y. Takeda, C. H. Hsu, F. C. Chuang, R. Laskowski, K. H. Khoo, A. Soumyanarayanan, and Y. Okada, Tailoring magnetism in self-intercalated Cr_{1+δ}Te₂ epitaxial films, *Phys. Rev. Mater.* **4**, 114001 (2020).
- [56] A. A. Soluyanov, D. Gresch, Z. Wang, Q. Wu, M. Troyer, X. Dai, and B. A. Bernevig, Type-II Weyl semimetals, *Nature (London)* **527**, 495 (2015).
- [57] B. Yan and C. Felser, Topological materials: Weyl semimetals, *Annu. Rev. Condens. Matter Phys.* **8**, 337 (2017).
- [58] M. Kang, S. Fang, L. Ye, H. C. Po, J. Denlinger, C. Jozwiak, A. Bostwick, E. Rotenberg, E. Kaxiras, J. G. Checkelsky, and R. Comin, Topological flat bands in frustrated kagome lattice CoSn, *Nat. Commun.* **11**, 4004 (2020).
- [59] L. Ye, M. Kang, J. Liu, F. von Cube, C. R. Wicker, T. Suzuki, C. Jozwiak, A. Bostwick, E. Rotenberg, D. C. Bell, L. Fu, R. Comin, and J. G. Checkelsky, Massive Dirac fermions in a ferromagnetic kagome metal, *Nature (London)* **555**, 638 (2018).
- [60] J.-X. Yin, S. S. Zhang, G. Chang, Q. Wang, S. S. Tsirkin, Z. Guguchia, B. Lian, H. Zhou, K. Jiang, I. Belopolski, N. Shumiya, D. Multer, M. Litskevich, T. A. Cochran, H. Lin, Z. Wang, T. Neupert, S. Jia, H. Lei, and M. Z. Hasan, Negative flat band magnetism in a spin-orbit-coupled correlated kagome magnet, *Nat. Phys.* **15**, 443 (2019).
- [61] Y. Tian, L. Ye, and X. Jin, Proper scaling of the anomalous Hall effect, *Phys. Rev. Lett.* **103**, 087206 (2009).
- [62] L. Wang, Q. Feng, Y. Kim, R. Kim, K. H. Lee, S. D. Pollard, Y. J. Shin, H. Zhou, W. Peng, D. Lee, W. Meng, H. Yang, J. H. Han, M. Kim, Q. Lu, and T. W. Noh, Ferroelectrically tunable magnetic skyrmions in ultrathin oxide heterostructures, *Nat. Mater.* **17**, 1087 (2018).
- [63] G. Zhang, F. Guo, H. Wu, X. Wen, L. Yang, W. Jin, W. Zhang, and H. Chang, Above-room-temperature strong intrinsic ferromagnetism in 2D van der Waals Fe₃GaTe₂ with large perpendicular magnetic anisotropy, *Nat. Commun.* **13**, 5067 (2022).
- [64] H. Deiseroth, K. Aleksandrov, C. Reiner, L. Kienle, and R. Kremer, Fe₃GeTe₂ and Ni₃GeTe₂: Two new layered transition-metal compounds: Crystal structures, HRTEM investigations, and magnetic and electrical properties, *Eur. J. Inorg. Chem.* **2006**, 1561 (2006).
- [65] Z. Li, H. Zhang, G. Li, J. Guo, Q. Wang, Y. Deng, Y. Hu, X. Hu, C. Liu, M. Qin, X. Shen, R. Yu, X. Gao, Z. Liao, J. Liu, Z. Hou, Y. Zhu, and X. Fu, Room-temperature sub-100 nm Neel-type skyrmions in non-stoichiometric van der Waals ferromagnet Fe_{3-x}GaTe₂ with ultrafast laser writability, *Nat. Commun.* **15**, 1017 (2024).
- [66] C. Liu, S. Zhang, H. Hao, H. Algaidi, Y. Ma, and X.-X. Zhang, Magnetic skyrmions above room temperature in a van der Waals ferromagnet Fe₃GaTe₂, *Adv. Mater.* **36**, 2311022 (2024).
- [67] B. Ding, Z. Li, G. Xu, H. Li, Z. Hou, E. Liu, X. Xi, F. Xu, Y. Yao, and W. Wang, Observation of magnetic skyrmion bubbles in a van der Waals ferromagnet Fe₃GeTe₂, *Nano Lett.* **20**, 868 (2020).
- [68] T.-E. Park, L. Peng, J. Liang, A. Hallal, F. S. Yasin, X. Zhang, K. M. Song, S. J. Kim, K. Kim, M. Weigand, G. Schutz, S. Finizio, J. Raabe, K. Garcia, J. Xia, Y. Zhou, M. Ezawa, X. Liu, J. Chang, H. C. Koo *et al.*, Néel-type skyrmions and their current-induced motion in van der Waals ferromagnet-based heterostructures, *Phys. Rev. B* **103**, 104410 (2021).
- [69] K.-X. Zhang, H. Ju, H. Kim, J. Cui, J. Keum, J.-G. Park, and J. S. Lee, Broken inversion symmetry in van der Waals topological ferromagnetic metal iron germanium telluride, *Adv. Mater.* **36**, 2312824 (2024).
- [70] A. Fert, N. Reyren, and V. Cros, Magnetic skyrmions: Advances in physics and potential applications, *Nat. Rev. Mater.* **2**, 17031 (2017).
- [71] <https://osf.io/>
- [72] DOI: [10.17605/OSF.IO/UFWGT](https://doi.org/10.17605/OSF.IO/UFWGT)